Journal Pre-proofs

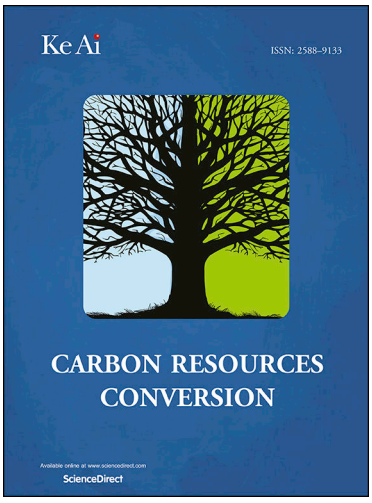

Original Article

Green Synthesis of biocompatible Gd^{3+}-doped Ultrasmall Carbon-based Nanohybrids from Coffee Wastes

Konstantin Paliienko, Anna Topchylo, Sergei Alekseev, Alain Géloën, Yurii Milovanov, Tetiana Lysenko, Valeriy Skryshevsky, Tatiana Borisova, Vladimir Lysenko

PII: S2588-9133(23)00068-6
DOI: https://doi.org/10.1016/j.crcon.2023.09.001
Reference: CRCON 197

To appear in: *Carbon Resources Conversion*

Received Date: 2 August 2023
Revised Date: 2 September 2023
Accepted Date: 10 September 2023

Please cite this article as: K. Paliienko, A. Topchylo, S. Alekseev, A. Géloën, Y. Milovanov, T. Lysenko, V. Skryshevsky, T. Borisova, V. Lysenko, Green Synthesis of biocompatible Gd^{3+}-doped Ultrasmall Carbon-based Nanohybrids from Coffee Wastes, *Carbon Resources Conversion* (2023), doi: https://doi.org/10.1016/j.crcon.2023.09.001

Green Synthesis of biocompatible Gd^{3+}-doped Ultrasmall Carbon-based Nanohybrids from Coffee Wastes

Konstantin Paliienko[a,b*], Anna Topchylo[c], Sergei Alekseev[d], Alain Géloën[e], Yurii Milovanov[b,c], Tetiana Lysenko[a,b], Valeriy Skryshevsky[b,c], Tatiana Borisova[a] and Vladimir Lysenko[f]

a. Department of Neurochemistry, Palladin Institute of Biochemistry, National Academy of Sciences of Ukraine; 9 Leontovicha str, Kyiv, 01054, Ukraine

b. Corporation Science Park, Taras Shevchenko University of Kyiv, 60 Volodymyrska Str., Kyiv, 01033, Ukraine

c. Institute of High Technologies, Taras Shevchenko National University of Kyiv, Volodymyrska Street, 64, 01601 Kyiv, Ukraine

d. Faculty of Chemistry, Taras Shevchenko National University of Kyiv, 64, Volodymyrs'ka St., 01601 Kyiv, Ukraine

e. UMR Ecologie Microbienne Lyon (LEM), CNRS 5557, INRAE 1418, Claude Bernard University of Lyon, VetAgro Sup, Research Team "Bacterial Opportunistic Pathogens and Environment" (BPOE), University of Lyon, F-69622 Villeurbanne, France

f. Light Matter Institute, UMR-5306, Claude Bernard University of Lyon/CNRS, Université de Lyon, 69622, Villeurbanne Cedex, France

* Corresponding authors at: Palladin Institute of Biochemistry, 9 Leontovicha Str., 01054, Kyiv, Ukraine.

E-mail address: kostyaram@gmail.coml, Tel: +38044 2343254

Highlights

- Ultra-small Gd-doped carbon dots can be synthesized from coffee wastes
- The synthesis corresponds to the basic green principles
- Gd-doped carbon dots exhibit superior properties of proton relaxation
- Gd^{3+} ions incorporation into the carbon dots enhances MRI contrast
- Carbon dots from coffee wastes are composed of carbohydrate polymers

Abstract

A cheap method allowing fabrication of biocompatible, ultra-small (2-10 nm) and fluorescent (λ_{em} = 425-500 nm) nanohybrids (NHs) from coffee wastes is reported. The

gadolinium-doped nanohybrids (GDNHs) or gadolinium-free carbon dots (GFCDs) can be synthesized in a domestic microwave oven according to green synthesis principles. Hydrodynamic sizes, chemical composition, impact on proton magnetic resonance relaxation time and optical properties of the GDNHs and GFCDs were studied in details and compared. In particular, doping of the NHs with Gd^{3+} ions, up to 1.87 % w/w of gadolinium per particles' weight, will allow their application for magnetic resonance imaging (MRI). Furthermore, cell culture tests on human adenocarcinomic alveolar basal epithelial cells line (A549) have shown high biocompatibility of the GDNHs and in a wide concentration range 100-1000 μg/ml.

Key words

Carbon dots from coffee waste

Carbon dots for MRI

Gadolinium-doped carbon dots

Microwave-assisted synthesis

1. Introduction

Carbon-based nanomaterials are a huge subgroup of nanosized materials including graphene and its derivatives (graphene oxide, graphane, graphone, graphyne, their allotropic modifications of different shape, such as: nanoribbons, nanosheets, nanotubes (single-, double- and multi-walled), holey carbon, fullerenes (buckyballs)), nanodiamonds [1–3] as well as large diversity of carbon dots (CDs) [4,5]. The CDs have sparked a special interest among all other carbon-based nanomaterials because of their unique properties, multidisciplinary applications, as well as extremely cheap and simple production methods [6].

There exist a lot of synthesis approaches to produce CDs, e.g.: pyrolytic, electrochemical, hydrothermal, solvothermal, laser-ablation etc. [5] Nowadays, the world's tendency strives to use economically efficient and safest technologies. In particular, various green synthesis concepts are being developed [7] and production of the CDs is not an exception. According to the great principles of green synthesis, biowastes treated with microwave energy appear to be the best feedstock to produce CDs [5,7]. As a source of biowastes there were used stunning variety of products e.g., fruit and vegetables peels (chestnut and peanut shells [8], durian [9], onion [10], garlic [11], sweet potato [12]), wheat straw [13], rice residue [14], fenugreek seeds [15], sugar cane molasses etc. [16] Coffee-based waste is one of the most easily accessible natural sources, which was also already considered for production of the CDs [17–21].

Waste-derived CDs are very promising for a variety of applications: sensorics, catalysis, drug delivery, bioimaging, diagnostics and therapy [6]. One of the most powerful bioimaging techniques is a magnetic resonance imaging or MRI diagnostic. For MRI diagnostics the lanthanide ions are usually applied as the contrast agents [22]. Nevertheless, the lanthanide salts are quite toxic for living organisms [23–25]. Thus, several attempts were done to make less toxic contrast agents based on CDs doped with lanthanides: Eu^{3+} [26,27], Tb^{3+} [28,29] and La^{3+} [30]. Among all lanthanides, gadolinium (3+) is the most appropriate ion for the MRI, because it has the highest magnetic moment and longest electron spin relaxation time (10^{-9} s) [31], which provides the best contrast MRI image after use. One can find several evidences of gadolinium incorporation into CDs, that were produced from commercial synthetic chemicals with help of energetically

unfavorable hydrothermal treatment [32–35], or with more adopted microwave-assisted method [36]. However, all of them are economically unprofitable with additional expenditures. In turn, we have not found any methods of CDs production from coffee wastes with Gadolinium incorporation.

In this paper, microwave-assisted green synthesis of Gd^{3+}-free CDs (GFCDs) and Gd^{3+}-doped carbon-based nanohybrids (GDNHs) from coffee wastes is reported for the first time. We focused on carrying out multistage purification, which usually does not draw sufficient attention in other publications. A special attention is paid to study an impact of Gd^{3+} ions on size distribution, surface chemistry and optical properties of the GDNHs in comparison with the Gd^{3+}-free CDs obtained from the same coffee waste sources. The main goal of our work was to synthesize ultra-small nontoxic carbon-based nanomaterial, which will be able to ensure good contrast in magnetic resonance imaging (MRI).

2. Materials and Methods

2.1 Materials and reagents

Coffee powder cake formed from original grinded coffee (Casa Del Caffé Vergnano S.P.A., Italia) in a kitchen coffee machine was used as a source of coffee wastes. The $GdCl_3 \cdot 6H_2O$ and $EuCl_3 \cdot 6H_2O$ salts, 25% (wt) NH_3 aqueous solution were purchased from Sigma-Aldrich™. The concentrators Vivaspin 20® with polyethersulfone (PES) membranes were purchased from Sartorius™. Dialyzing sacks were made of membrane with nominal filter rating 3’500 MWCO (ZelluTrans ROTH® Regenerated Cellulose Tubular Membrane, flat width 19 mm, wall thickness 25 µm, volume per length 1,15 ml/cm). All other chemicals of analytical grade were purchased from Fluka, Germany, and used without further purification. The ultrapure water with specific resistance 18.2 MΩ·cm was used during all processes.

2.2 Synthesis of nanohybrids from coffee

Carbon-based Gd^{3+}-doped nanohybrids (GDNHs) were prepared according to the scheme shown in Fig. 1.

In Step 1, the used coffee cake from the coffee machine was collected and dried in air at 130 °C for 120 min in a glass evaporating dish on the hotplate. In Step 2, for GDNHs synthesis 5 g of the dried coffee cake was refluxed with 15 ml of 0.1M $GdCl_3$ in a 50 ml round-bottom flask for 50 min at 100 °C, heated under the hotplate. For the GFCDs synthesis, this step was performed identically, with 15 ml of water instead of $GdCl_3$ solution.

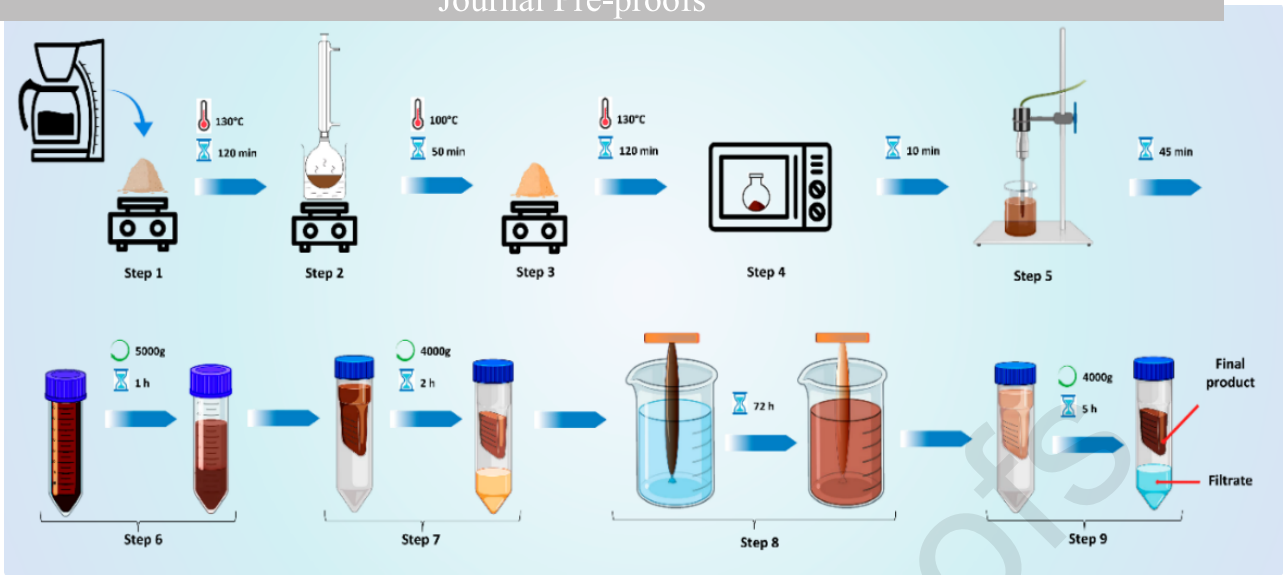

Fig. 1. Fabrication scheme of the coffee-based nanohybrids. Step 1 – Preliminary drying; Step 2 – Preliminary treatment and incorporation of Gd; Step 3 – Drying; Step 4 – Carbonization; Step 5 – Sonication; Step 6 – Debris elimination; Step 7 – Elimination of large nanoparticles; Step 8 – Dialysis; Step 9 – Preconcentration.

Then, in Step 3, the treated biomass was dried in air at 130 °C for 120 min. In Step 4, the dried biomass was mixed with 10 ml of 10 % (wt) aqueous NH_3 in a 250 ml round-bottom flask, and the mixture was heated in a domestic microwave oven (700W consumption power) for 10 min. In Step 5, the sintered biomass was placed into a 50 ml glass beaker and thoroughly suspended in 20 ml of water. The formed suspension was sonicated for 45 min at 100 % of total power with Ultrasonic dispergator (Bandelin electronic, GM 2070 model, 70-Watt, 20 kHz). Then the ultrasonicated suspension was centrifuged at 5'000g for 1 hour in 50 ml centrifuge tubes to eliminate coarse coffee debris (Step 6). At Step 7 the supernatant solution from Step 6 was placed into ultra-filtration spin columns (or concentrators) Vivaspin 20® (30'000 MWCO, PES membrane) and centrifuged at 4'000g for 2 hours. Step 8 is the longest step taking 72 hours. All liquid passed through the 30'000 MWCO membrane was collected and placed into dialyzing sacks 20 cm of length with membrane's pores of 3'500 MWCO. Dialyzing sacks filled with GFCDs and GDNHs were put separately into 1000 ml beakers with 650 ml of water in each. Water in beakers was refreshed each 12 hours for 72 hours. Last Step 9 includes preconcentration of GFCDs and GDNHs carbon dots via centrifugation of dialyzed solutions through 3'000 MWCO Vivaspin 20® PES membranes at 4'000g; 2 hours is sufficient for GDNHs, while approximately 5 hours is needed for GFCDs. The stock concentrated solutions over the membranes are named GDNHs (with gadolinium) in a final volume of 4 ml and GFCDs (without gadolinium) in a final volume of 5 ml. Additionally, Eu^{3+}-doped nanohybrids EuDNHs were synthesized by the identical protocol as GDNHs and used only in ^{1}H-NMR analysis. Concentrations of the solutions were determined gravimetrically by freeze-drying and then heating with 1 ml of acetone in 2 ml glass beakers at 105 °C on hotplate for 2 hours. Dry mass content found to be 14.1 mg/ml) for the GFCDs (pH 4.55), and 37.3 mg/ml for the GDNHs (pH 5.16).

Additionally, Gd content was determined by ICP-MS analysis using a Perkin Elmer NexION2000. Measurements were performed in kinetic energy discrimination (KED) mode. Calibration curve was built using PlasmaCAL® Gd standard for ICP-AES and -MS analysis. The samples are prepared by dilution in 1 % v/v HNO_3 solution. No traces of gadolinium were found in the GFCDs sample, while the GDNHs sample contains 1.87 % w/w of gadolinium per mass of dried particles.

2.3 Post-synthesis characterization techniques

Proton magnetic resonance relaxation time T_1 was measured by Bruker Minispec MQ60 nuclear magnetic resonance analyzer (Bruker, USA), operating at 37 °C under 1.4 T (60 MHz) magnetic field. Aliquots of 300 µl were taken from concentrated samples and measured in special glass vials.

Size distribution measurements of diluted colloidal solutions of the GDNHs and GFCDs were performed using Zetasizer Nano ZS from Malvern Instruments (He–Ne laser 633 nm, 5mW, with 173° Non-Invasive Back Scatter (NIBS) detector and narrow band filter).

Absorbance spectra of diluted colloidal solutions of GDNHs and GFCDs were recorded by means of UV–visible spectrophotometer Cary Eclipse Varian 50 Scan with wavelength range limits from 190 to 1100 nm. Measurements were performed in UV Quartz SUPRASIL® cuvette (B0631009, 10mm light path, 3.5ml volume).

^{1}H-NMR (proton nuclear magnetic resonance) was performed on Bruker NanoBay 400 MHz. The sequence program is zg90 (90° pulse to maximize the emitted signal), 64 scans and Acquisition time (AQ) = 4 sec. Lyophilized samples without metals and Europium-doped sample were redispersed in deuterium oxide D_2O with a final concentration of 6 mg/ml.

FTIR (Fourier-transform infrared) spectra of the lyophilized samples were acquired on IRAffinity-1, Shimadzu® in attenuated total reflection (ATR) mode, using PIKE MIRacle™ ATR platform (diamond crystal plate). Dried amorphous powders of the lyophilized samples were allocated on a crystal plate, the spectra (32 scans) in 600 - 4000 cm^{-1} range with a resolution of 0.5 cm^{-1} in Happ-Genzel apodization mode were recorded and analyzed with Shimadzu IR solution v1.50®.

Fluorescent properties of the samples were studied on Cary Eclipse spectrofluorimeter from Agilent. This spectrofluorimeter is equipped with a 75 kW Xenon flash lamp with Δpulse = 2 µs, two Czerny-Turner type monochromators and an 800 V PM detector. The lamp frequency is set to 100 Hz by default.

2.4 Biocompatibility assessment of nanohybrids

Cell biocompatibility of the GDNHs and GFCDs was analyzed by means of a non-destructive impedance-based method (xCELLigence, ACEA Biosciences Inc., Biotek, Colmar, France), that has been successfully applied for carbon nanomaterials toxicity assessment [37]. By inspecting a cell index of human carcinoma A549 cell line (provided by ATCC, Massanas, VA, USA), it is possible to conclude about compatibility of nanohybrids within the cells (see Fig. S1). Detailed description of procedures and results are available in the Supplementary Information part. Furthermore, a comparative multi-level toxicity assessment of these nanohybrids was recently conducted and published [38].

3. Results and discussion

3.1 Relaxometry

In order to be sure of successful synthesis of GDNHs, two main points must be checked: (i) whether free Gd^{3+}-ions are still present in the final GDNHs sample and (ii) is the gadolinium sufficiently strongly complexed with the carbon dots. The GFCDs were used as the control sample. One can evaluate content of Gd^{3+} in a sample [39], conclude about samples' purity and success of gadolinium incorporation by measuring longitudinal proton relaxation times (T_1). To evaluate the quality of dialysis and overall purification process, the relaxometry technique was applied (Fig. 2).

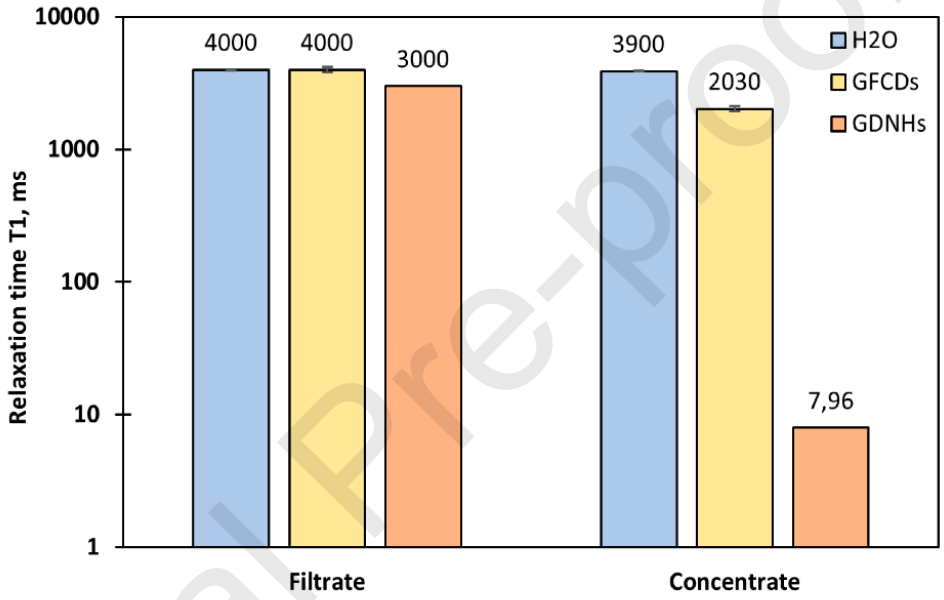

Fig. 2. Relaxation times T_1 of the filtrates and concentrates of GDNHs and GFCDs samples. T_1 value of water was measured each time for control.

First, as one can see in Fig. 2, T_1 values of pure water remain constant (4000 ± 100 ms) meaning that the measurements were accurately conducted. After preconcentration of GFCDs (see Fig. 1, Step 9), the relaxation time of the filtrate passed through 3'000 Da membrane is equal to 4000 ± 100 ms as for water. Relatively slight decrease of T_1 in the GFCDs concentrate (2030 ± 20 ms) could be explained by some GFCDs paramagnetism, caused by the presence of unpaired electrons as organic free radicals. Indeed, relatively stable paramagnetic organic radicals such as high-spin polymer radicals [40] and dimerized small organic radicals [41] could exist even at room temperature.

Compared to the relaxation times of the GFCDs filtrate, T_1 of GDNHs filtrate is slightly decreased (3000 ± 100 ms) due to presence of traces of some free Gd^{3+}-ions (<6 ppm). Meanwhile, T_1 of GDNHs concentrate is dramatically reduced (7.96 ± 0.03 ms) and indicates the presence of a high quantity of gadolinium-doped nanohybrids with molecular weight above 3'500 Da, which cannot (contrary to Gd^{3+}-ions) pass through the 3'000 Da filter. The MRIs of the GFCDs

and GDNHs samples localized in a mouse phantom are shown in Fig. S2 and discussed in the Supplementary part. A perfect correlation with the results described above and shown in Fig. 2 can be stated.

3.2 Dynamic light scattering analysis

Hydrodynamic size distributions of the carbon dots were determined using dynamic light scattering (DLS) technique as shown in Fig. 3.

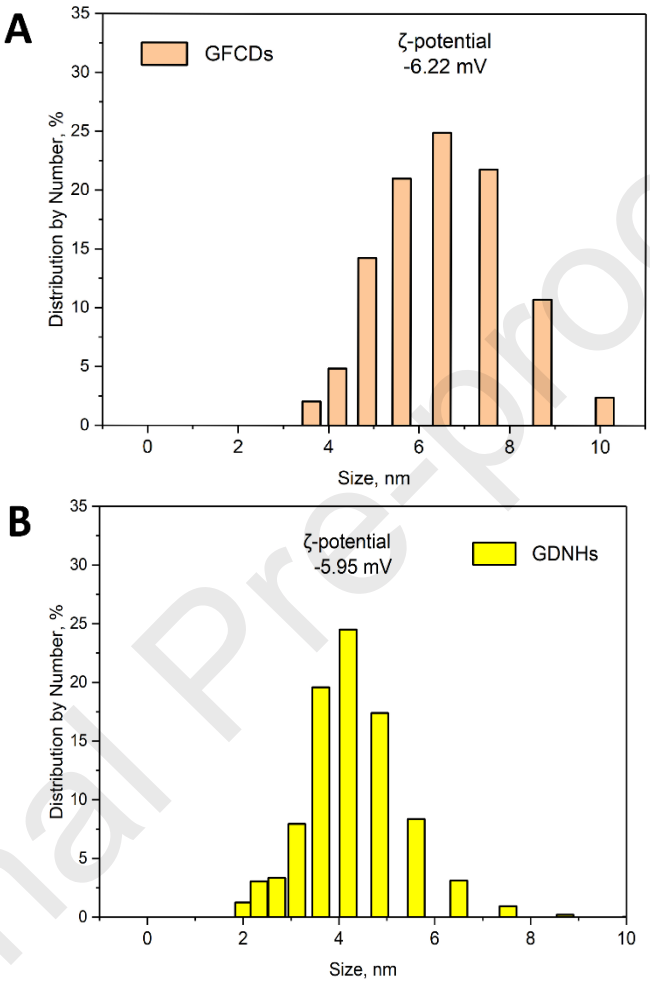

Fig. 3. Cumulative diagram of DLS analysis of GFCDs (A) and GDNHs (B). Measurements for each sample were performed 5 times repeating 50 runs for 10 seconds.

The samples were examined after dilution to 200 μg/ml in water (to avoid agglomeration of the CDs leading to overestimation of their size distribution) followed by pH adjustment with 10 mM NaOH to 7.4 as a common value for biological environment. As one can see, both samples are characterized by ultra-small sizes < 10 nm. The GFCDs sample is characterized by a slightly larger size distribution in the 4-11 nm range, while the GDNHs sample is appeared to be more uniform and smaller, having a 2-7 nm size distribution. In addition, Z-potentials measured at pH 7.4 appeared to be -6.22 and -5.95 mV for GFCDs and GDNHs, respectively.

3.3 UV-VIS absorption spectroscopy

Typical absorbance spectra of the GFCDs and GDNHs samples in aqueous solutions (200 μg/ml) are shown in Fig. 4. Black points on the insets correspond to initially obtained UV-VIS absorption spectra. After subtraction of exponential-like baselines (the blue lines shown on the insets) representing enhanced optical absorption especially in the spectral range 4.5-6.0 eV due to π–>π* transitions in sp^2-hybridized carbon domains (C=C), one can get complex multicomponent spectra (red lines) with clearly visible spectral features. Deconvolution of the obtained spectra on elementary Gaussian-like peaks (see Fig. 4) allows us to understand better how incorporation of Gd^{3+} ions impacts the UV-VIS absorption of studied carbon nanohybrids. First, one can state that the relative absorbance of the GDNHs samples is higher in the whole spectral range. Second, the incorporation of Gd^{3+}-ions leads to disappearance of the peak 6 in the spectrum of GDNHs sample.

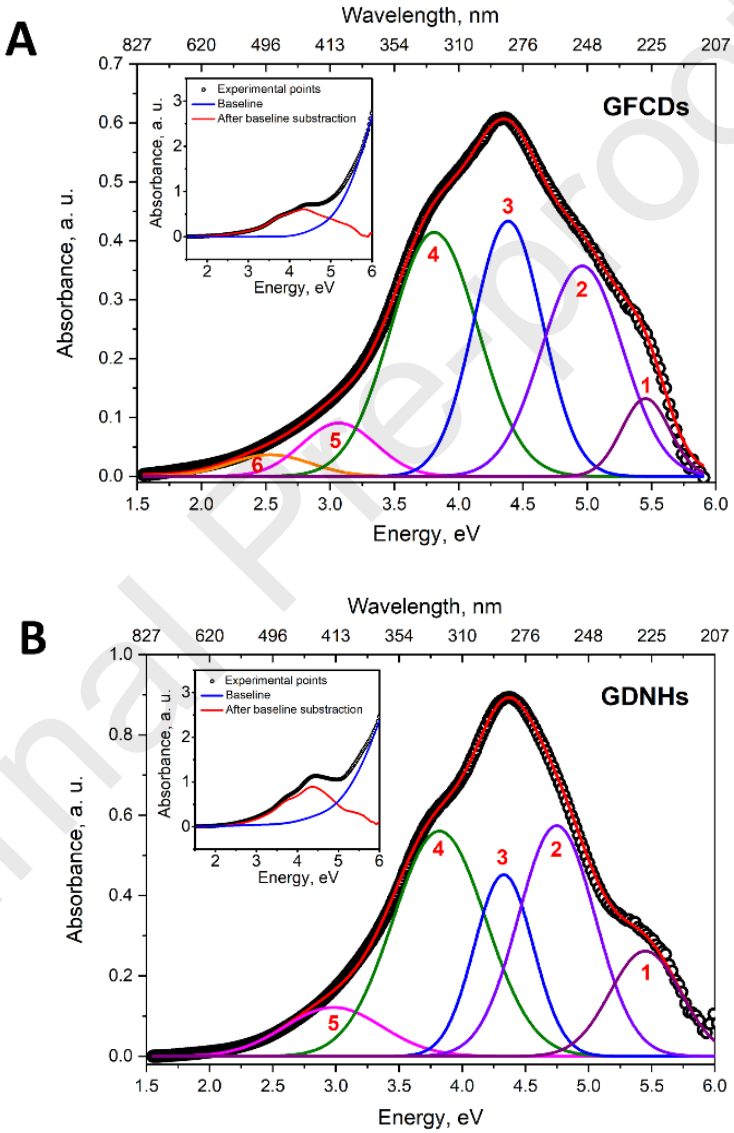

Fig. 4. UV-VIS absorption spectra the GFCDs (A) and GDNHs (B) samples.

According to the literature data, the high-energy bands (1-3) correspond to π–>π* transitions involving aromatic sp^2 carbons (aromatic C=C bonds). The next two bands (4, 5) can be assigned to the intrinsic absorption of n–>π* transitions of the C=O/C=N bonds in carbon cores. The absorption bands below 3 eV originate from the surface state transitions [42]. It worth

noting that the n–>π* transitions and the broad surface-state absorption bands are usually overlapped. Thus, the band 5 can be also associated to a photo-induced electronic transition in a surface chemical bond. As for the band 6, it can be attributed either to the addition of nitrogen into the carbon sp^2 lattice or to the surface states involving nitrogen, that correlates well with higher content of nitrogen in GFCDs according to an EDX analysis (Fig. S5).

3.4 Fluorescence excitation/emission maps

Excitation/emission fluorescence (FL) maps of the colloidal solutions containing GFCDs and GDNHs are shown in Fig. 5-(A) and 5-(B), respectively.

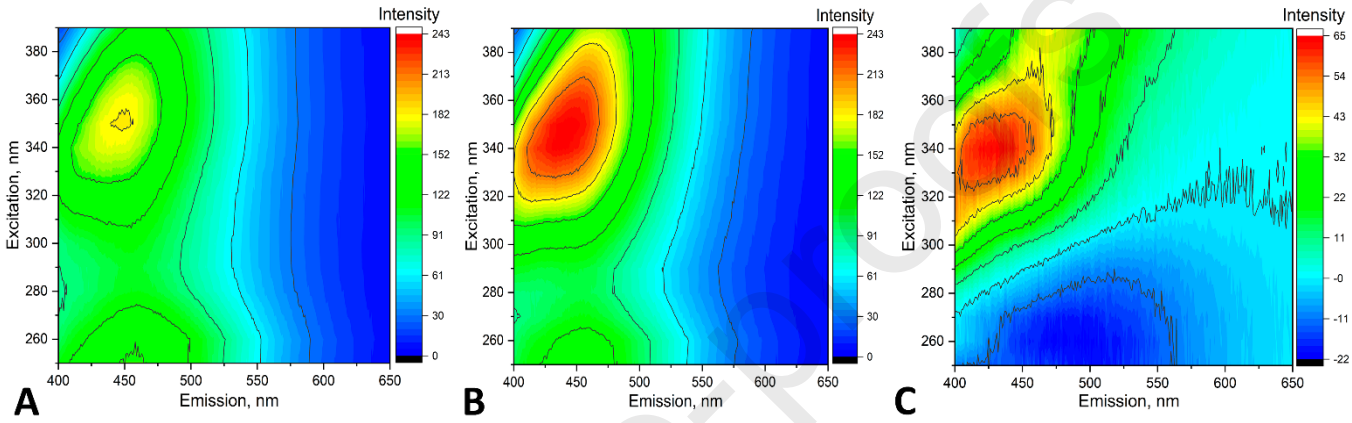

Fig. 5. Fluorescence excitation/emission spectra of GFCDs (A), GDNHs (B) and their comparative subtraction difference (C).

A characteristic blue emission band (410-475 nm) resonantly excited in the spectral range 340-370 nm can be clearly observed. As one can see, the maximum intensity of fluorescence emission of the GDNHs samples is higher compared to the FL intensity of the GFCDs samples. It can be at least partially explained by the higher absorbance level of the GDNHs samples in the spectral range 330-370 nm (3.35-3.75 eV) as reported above (see Fig. 4). In order to emphasize the spectral difference between the excitation/emission maps of GFCDs and GDNHs, their subtraction is shown in Fig. 5-(C). It allows visualization of spectral regions where the intensity difference is the most pronounced. As a result, the GDNHs solutions are more fluorescent in blue spectral region centered at 425 nm when excited at 340 nm, while fluorescence intensity of the GFCDs solutions is higher in green spectral region centered near 500 nm when excited at 260 nm. In other words, incorporation of Gd^{3+}-ions into carbon dots leads to intensity suppression of green fluorescent carbon dots and to enhancement of photo-induced emission intensity of blue fluorescent species.

3.5 ^{1}H-NMR spectroscopy

It is known that Gd^{3+} ions are strongly paramagnetic and result in impossibility to get an informative ^{1}H-NMRs. Thus, it was decided to replace Gd^{3+} ions with Eu^{3+} ions. Europium is a lanthanide atom from the same group and with similar chemical properties as gadolinium, but in NMR analysis it works as a slight shift reagent [43] and can be successfully used for the analysis.

For the analysis of carbon-based nanohybrids two samples have been chosen: GFCDs – gadolinium-free carbon dots as a control and EuDNHs – europium-doped nanohybrids which

were produced from the same coffee cake and by the same synthesis protocol as used for GDNHs (Fig. 1). Obtained ^{1}H-NMR spectra are shown in Fig. 6.

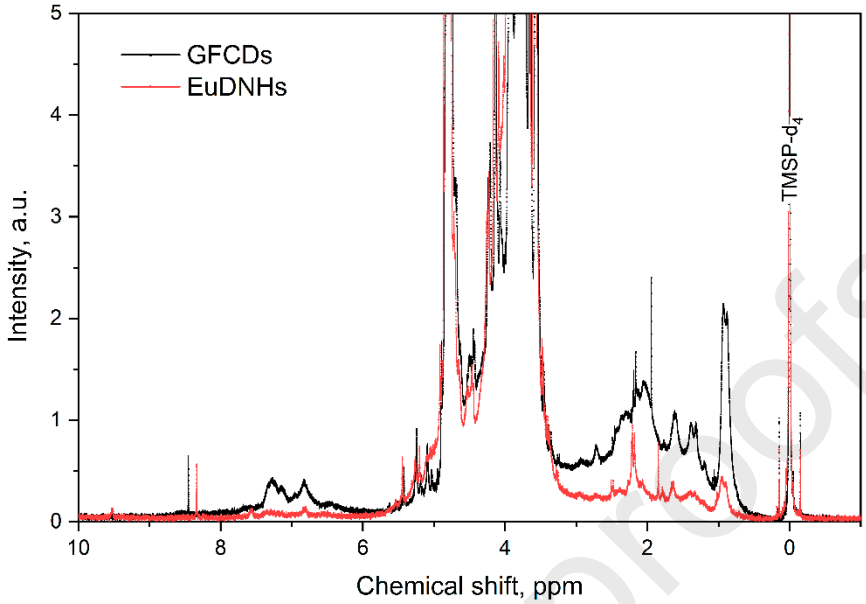

Fig. 6. 1H-NMR spectra of GFCDs and EuDNHs dispersed in D2O. TMSP-d4 is used as a reference compound. Transmitter frequency – 400 MHz, fid resolution – 0.24 Hz.

Strong singlets at 0.00 and 4.79 ppm are related to the reference compound and the solvent (HDO impurity in D_2O), respectively. The protons of hydroxyls and other "mobile" protons of the CDs are also included in the HDO signal due to their exchange with deuterium. The sample-related spectrum is very complex, composed of both narrow signals with well-defined thin structure and wide signals. It indicates decreased mobility of corresponding chemical groups within the particle.

There are three main regions in the spectra: (i) the signals at 0.5 – 3 ppm are related to the protons in various alkyl groups, (ii) 3 – 6 ppm range corresponds to CH–OH protons in carbohydrate fragments and to C=CH "olefin" protons, (iii) 6 – 8 ppm can be assigned to the protons in aromatic fragments. The singlet at 8.45 ppm (GFCDs) and 8.34 ppm (EuDNHs) can be related to the protons near unsaturated C-atoms e.g., benzene ring, aromatic system, etc. Fussy peaks at 7.28, 7.14, 6.96, 6.82 ppm are related to the protons of heterocyclic compounds. According to the spectral signals' intensities, the main part (3 – 6 ppm) of CDs is represented by complex carbohydrate moieties. More detailed spectrum of carbohydrate's region is presented in Fig. 7.

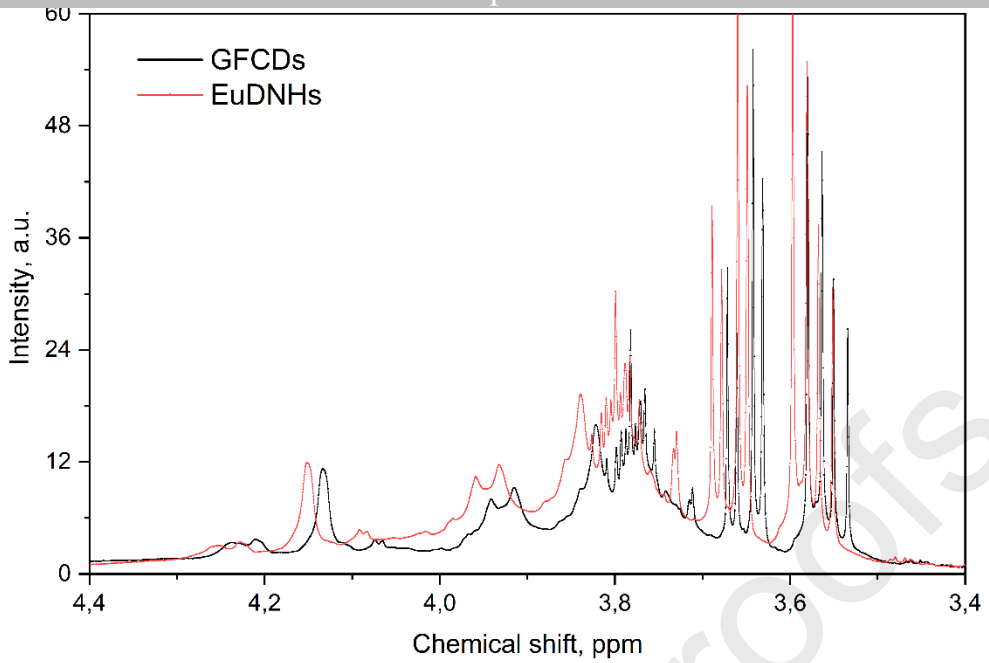

Fig. 7. Fragment of 1H-NMR spectra, depicted in Fig. 6, in the range from 3.4 to 4.4 ppm.

This part of the spectra of the both samples are very similar and may be referred to arabinan-like [44] structures. However, all peaks of the sample with Eu^{3+} are shifted approximately on 0.02 ppm to low field due to the action of Eu^{3+} as a lanthanide shift reagent. Small value of the shift points at a large distance between Eu^{3+} ions and C-H groups near oxygen of carbohydrate's part. At the same time, the shift between peaks 8.45 ppm and 8.34 ppm is more significant and occurred in a strong field for Eu-doped CDs in contrast to the carbohydrate's part. Presumably, Eu^{3+} ions (as well as Gd^{3+} ones) might be entrapped not by the main carbohydrate's part, but by the side chain elements inside the CDs. ^{1}H-NMR spectra of both samples indicate the presence of both alkyl and aromatic fragments. Being strong Lewis's acids, Eu^{3+} and Gd^{3+} cations coordinate to the carboxylates and phenolic groups of CDs.

3.6 FTIR spectroscopy

The Fig. 8 represents FTIR spectra of freeze-dried samples of GDNHs and GFCDs. The spectra of GDNHs and GFCDs are very similar to each other.

The main bands in their spectra are identical to those of carbohydrates. Specifically, it tends to be very similar to the structure of arabinogalactans [45–47]. Particularly, the wide band at 3400-3000 cm^{-1} corresponds to stretching vibrations ν(O–H) of hydrogen-bonded hydroxyls, medium-intensity bands at 3000-2800 cm^{-1} – to ν(C–H) of sp^3-hybridized alkane bonds, and the most intense band at 1024 cm^{-1} – to ν(C–O) of carbohydrates. The band centered at 1650 cm^{-1} can be composed by adsorbed water scissors (δ(H-O-H)), by asymmetrical stretches of ionic or Gd-coordinated carboxylate anions $\nu_{as}(-CO_2^-)$, C=O stretches of amides, quinones and other conjugated species, C=C stretches in aromatic rings and by other bands. The band at 1544 cm^{-1} could be related to C=N stretches in conjugated systems or to amide-II vibrations in polypeptide fragments. The band between 1420 and 1380 cm^{-1} arose due to deformation vibrations of C–H and O–H bonds in organic species and to deformations of NH_4^+-cation, also due to symmetrical stretches of the carboxylate $\nu_s(-CO_2^-)$ and some vibrations of aromatic fragments. The band at

1313 could be related to mono- and disubstituted amines with aromatic system. The band 1246 cm^{-1} could be attributed respectively to syringyl and guaiacyl units [48] or to chlorogenic acid fragments [49] inside the CDs. Region between 863 and 760 cm^{-1} shows presence of anomeric carbons of both pyran and furan ring configurations [50].

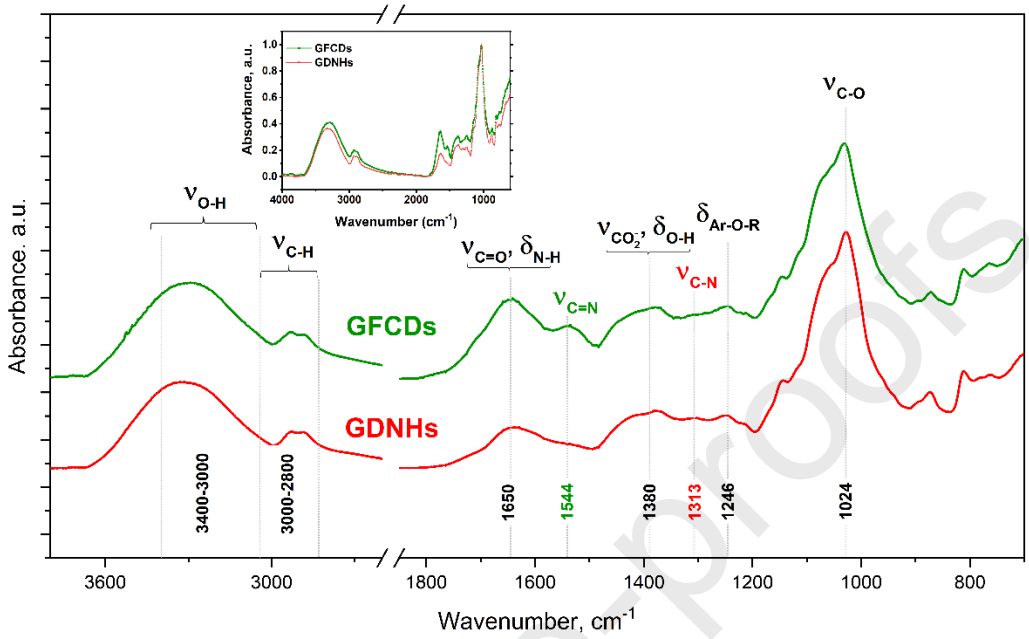

Fig. 8. FTIR spectra of GDNHs (red) and GFCDs (green) carbon dots. Break from 2600 to 1850 cm^{-1} contains insignificant region without any absorption bands. In the minimized window unprocessed spectra are shown.

Comparing the spectra of the CDs with and without gadolinium, one could see that intensities of the bands at 1650, 1544, 1380 and 1246 cm^{-1} are significantly lower for metal-containing samples (minimized window in Fig. 8). In accordance with ^{1}H-NMR and UV-vis data this difference can be explained by constriction of bonds vibrations in carboxylates and phenols due to complexation with metals, as well as being located inside the particle. At the same time metal-free CDs have a more pronounced C=N signal that could be related to more quantity of diketopiperazines and other nitrogen-based conjugated systems. Obviously, the metal ions residing in the CDs are coordinated to carboxylates, phenolic groups, and lone electron pair of nitrogen, while the main part of the CDs is composed of the carbohydrate chains, ensuring their solubility in aqueous media. Their structure should be similar to one of coffee melanoidins, forming under normal coffee brew [51].

3.7 Chemical structure of the carbon-based nanohybrids

Chemical composition of roasted coffee includes a big number of organic compounds with different solubility, such as: carbohydrates (cellulose, hemicellulose, and other poly- and monosaccharides), polyphenolic compounds (e.g., lignin and tannins), fats, proteins, caffeine, chlorogenic acids and other carboxylic acids [49,52]. A significant part of water-soluble carbohydrates (galactose, rhamnose, arabinose and uronic acids) is washed out already during the brewing process in the coffee machine. The remaining part of water-insoluble chemical substances mainly define the chemical composition of our carbon-based nanohybrids which is further affected by the technological steps described in Fig. 1. In particular, under boiling with a

reflux (Step 2) a lot of thermosensitive polysaccharides, proteins and lipids are decomposed into monomers. In the same time, chlorogenic acids, melanoidins, pectins and arabinogalactans [53] could be released and solubilized. Predominately arabinogalactan proteins undergo the decomposition into monomers, in contrast to mannans and cellulose which are very hard to extract under these conditions. After hydrolysis, the boiled slurry has relatively moderate acidity due to the presence of proton-donating species: uronic acids and their derivatives, chlorogenic acids (e.g., caffeic, ferulic, and p-coumaric acid as soluble esters of quinic acid), and also arabinogalactans (which contain 6-8 % of glucuronic acid monomers) [54]. Addition of $GdCl_3$ may lead to coordination of carboxylic domains across 9 available positions [55–57] which makes chlorogenic acids more reactive with respect to benzene ring, phenolic hydroxyls and double bonds. Without Gd^{3+} ions, carboxylic groups undergo esterification and amidation reactions. The drying of coffee cake (Step 3) results in settling of the extracted compounds on the surface of coffee grains.

Addition of 10 % NH_3 (aq.) to the dried coffee cake (Step 4) makes the whole reaction medium basic, ensures the anionic compounds to be more soluble, and dissolves the sedimented surface compounds. Furthermore, the basic medium converts sugars from cyclic to open chain configuration making them more reactive toward amino acids and other amino structures [58]. The more reactive sugars are present, the more Maillard and Amadori products as well as melanoidins appear. The microwave-induced heating leads to the evaporation of ammonia excess and consequently, the processes of polymerization and carbonization begin. It results in miscellaneous transformations of coffee chemical moieties. Taking into account literature data on hydrothermal carbonization of the carbohydrates [59] as well as the reactions of cellulose ammoxidation [60] or wood treatment [61] with NH_3, the following reactions should be taken into account: (i) condensation reactions, such as: Maillard reactions [51,62], and aldol condensation, (ii) alkylation of phenols, (iii) dehydration of the carbohydrates with formation of furan and pyrrole heterocycles. These reactions are followed by carbonization giving condensed aromatic and heteroaromatic domains [51], formation of amines derivatives, amides, esters and ammonium salts from carboxylic acids, and formation of Schiff bases from carbonyl compounds.

In several works [51,63] hydroxycinnamic acids (e.g., caffeic and ferulic) were proposed to be attached to the melanoidin's backbone through the non-ester linkage which correlates very well with our ^{1}H-NMRs spectral analysis. Moreover, based on our FTIR analysis, we deal with arabinogalactan-based carbon dots. Therefore, previously hydrolyzed phenolic acids bind metal atoms firstly, and then being chelated by carboxylic groups become linked through the phenolic part to the carbohydrate backbone under microwave annealing. In addition, for the Gd^{3+}-free CDs, the heterocyclic part (6.5 – 7.5 ppm of ^{1}H-NMR in Fig. 6, or 1544 cm^{-1} of FTIR in Fig. 8) is more pronounced. It could be explained by formation of diketopiperazines from hydrolyzed proteins [64]. Due to the very small hydrodynamic radius of the nanohybrids, arabinogalactan is supposed to be partially decomposed during ammoxidation. Nevertheless, metal-free carbon dots continue to be highly branched structures associated with amino acid residues from structural proteins [65]. The carboxylic moieties may cause electrostatic repulsion inside the structure of the GFCDs making it more "fluffy" and bulky (Fig. 9A-B) compared to the GDNHs.

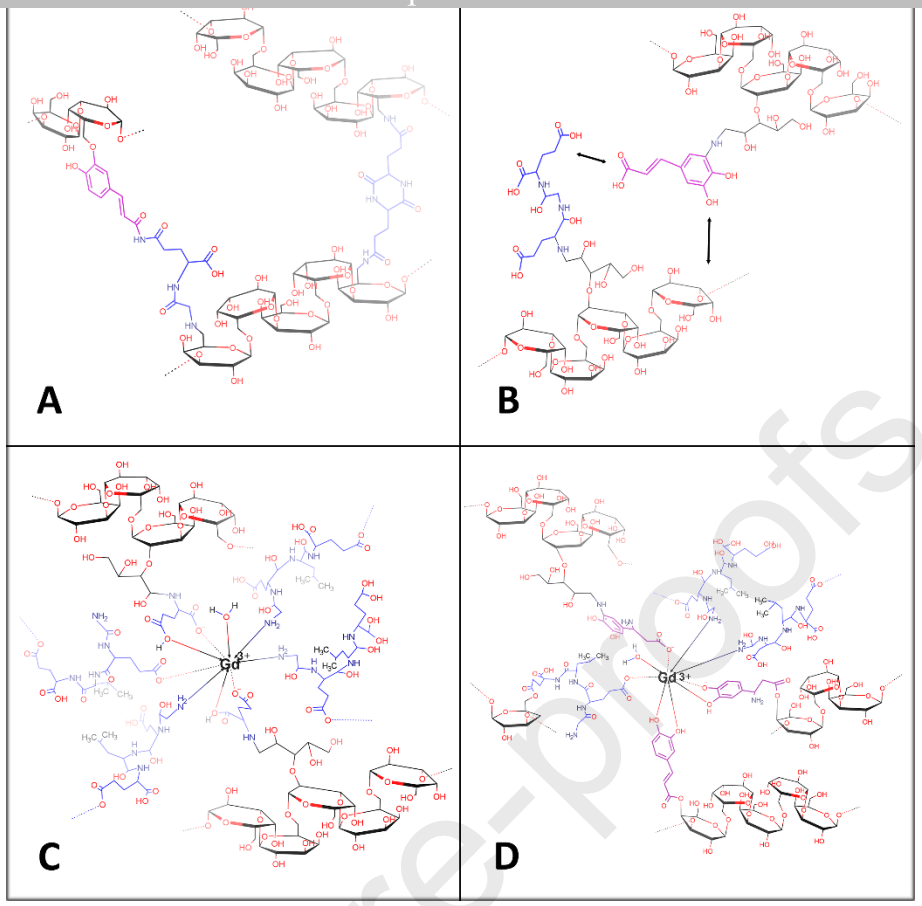

Fig. 9. Possible chemical formations in the Gd-free carbon dots associated with inner cross-linking (A) and repulsion (B). Specific domains in the Gd-doped nanohybrids participate in chelation of Gd^{3+} ions through amino acidic binding (C) and with hydroxycinnamic acid derivatives chelation (D). The drawings were made in Marvin Sketch v23.2, ChemAxon (http://www.chemaxon.com).

Absence of diketopiperazines from hydrolyzed proteins in the Gd^{3+}-doped nanohybrids may be due to involvement of free amino acids or terminal reactive groups of oligopeptides into donor-acceptor and ionic binding of metal atoms (e.g., glutamate, glycine and aspartate [66]). Additionally, hydroxyphenolic moieties of cinnamic acid derivatives, which distributed on arabinogalactan side-chains, could take part in coordination of Gd^{3+} ions, causing cross-linking of constituent molecules making GDNHs smaller in size and uniform (Fig. 9C-D).

4. Conclusions

Ultra-small Gd^{3+}-free CDs (GFCDs) and Gd^{3+}-doped carbon-based nanohybrids (GDNHs) were successfully fabricated from coffee wastes with the use of microwave-assisted green synthesis approaches. The samples are characterized by blue fluorescence in 410-475 nm range under UV excitation as well as possess paramagnetic Gd^{3+}-ions for MRI application. Global chemical composition of the GDNHs and GFCDs is quite similar. The both consist of carbohydrate skeleton (mainly arabinogalactan) with condensed aromatic and heteroaromatic domains, bearing various functional groups, mainly hydroxyl and carbonyl; to a lesser extent amide bonds and amino groups; and trace amounts of carboxyl groups are present. Additionally, complexation of Gd^{3+} ions occurs

through carboxylic and amino groups of oligopeptide fragments, as well as with help of carboxylic and hydroxyl groups of cinnamic acid derivatives making structure of nanohybrids stable, compact and uniform.

Besides the multimodal functionalities, the both samples occurred to be non-toxic for human carcinoma A549 cell line in the range of concentrations from 0.1 to 1 mg/ml, that equals to the ratio: 100 μg of carbon dots per 2500 cells.

In future, bio-distribution of the nanohybrids will be studied in-vivo by MRI facilities.

CRediT authorship contribution statement

Conceptualization, K.P., T.B. and V.L.; Methodology, K.P. and V.L.; Formal analysis, K.P., V.L. and S.A.; Investigation, K.P., A.T., A.G., Y.M., S.L. and T.L.; Data curation, K.P. and V.L.; Writing – Original Draft preparation, K.P.; Visualization, K.P.; Supervision, V.L., V.S. and T.B.; Writing – Reviewing and Editing, V.L., S.A.; Funding acquisition, V.S. All authors have read and agreed to the published version of the manuscript.

Declaration of Competing Interest

The authors declare that they have no known competing financial interests or personal relationships that could have appeared to influence the work reported in this paper.

Acknowledgements

All authors of this work acknowledge the support of EU Horizon 2020 Research and Innovation Staff Exchange Programme (RISE) under Marie Skłodowska-Curie Action (project 101008159 “UNAT”).

References

[1] S.K. Debnath, R. Srivastava, Drug Delivery With Carbon-Based Nanomaterials as Versatile Nanocarriers: Progress and Prospects, Front. Nanotechnol. 3 (2021) 15. https://doi.org/10.3389/FNANO.2021.644564/BIBTEX.

[2] E. Alfaro, A.B. Engin, D. Holmannova, P. Borsky, T. Svadlakova, L. Borska, Z. Fiala, Reproductive and Developmental Nanotoxicity of Carbon Nanoparticles, Nanomater. 2022, Vol. 12, Page 1716. 12 (2022) 1716. https://doi.org/10.3390/NANO12101716.

[3] M.A. Torkaman-Asadi, M.A. Kouchakzadeh, Atomistic simulations of mechanical properties and fracture of graphene: A review, Comput. Mater. Sci. 210 (2022) 111457. https://doi.org/10.1016/J.COMMATSCI.2022.111457.

[4] B. Wang, S. Lu, The light of carbon dots: From mechanism to applications, Matter. 5 (2022) 110–149. https://doi.org/10.1016/J.MATT.2021.10.016.

[5] C. He, P. Xu, X. Zhang, W. Long, The synthetic strategies, photoluminescence mechanisms and promising applications of carbon dots: Current state and future perspective, Carbon N. Y. 186 (2022) 91–127.

https://doi.org/10.1016/J.CARBON.2021.10.002.

[6] H. Salimi Shahraki, A. Ahmad, R. Bushra, Green carbon dots with multifaceted applications– Waste to wealth strategy, FlatChem. 31 (2022) 100310. https://doi.org/10.1016/J.FLATC.2021.100310.

[7] O. V. Kharissova, B.I. Kharisov, C.M.O. González, Y.P. Méndez, I. López, Greener synthesis of chemical compounds and materials, R. Soc. Open Sci. 6 (2019). https://doi.org/10.1098/RSOS.191378.

[8] F. Mancini, A. Menichetti, L.D. Esposti, M. Montesi, S. Panseri, G. Bassi, M. Montalti, L. Lazzarini, A. Adamiano, M. Iafisco, Fluorescent Carbon Dots from Food Industry By-Products for Cell Imaging, J. Funct. Biomater. 2023, Vol. 14, Page 90. 14 (2023) 90. https://doi.org/10.3390/JFB14020090.

[9] J. Praneerad, K. Neungnoraj, I. In, P. Paoprasert, Environmentally Friendly Supercapacitor Based on Carbon Dots from Durian Peel as an Electrode, Key Eng. Mater. 803 (2019) 115–119. https://doi.org/10.4028/WWW.SCIENTIFIC.NET/KEM.803.115.

[10] K. Bankoti, A.P. Rameshbabu, S. Datta, B. Das, A. Mitra, S. Dhara, Onion derived carbon nanodots for live cell imaging and accelerated skin wound healing, J. Mater. Chem. B. 5 (2017) 6579–6592. https://doi.org/10.1039/C7TB00869D.

[11] P. Das, S. Ganguly, P.P. Maity, H.K. Srivastava, M. Bose, S. Dhara, S. Bandyopadhyay, A.K. Das, S. Banerjee, N.C. Das, Converting waste Allium sativum peel to nitrogen and sulphur co-doped photoluminescence carbon dots for solar conversion, cell labeling, and photobleaching diligences: A path from discarded waste to value-added products, J. Photochem. Photobiol. B Biol. 197 (2019) 111545. https://doi.org/10.1016/J.JPHOTOBIOL.2019.111545.

[12] H. Liu, L. Ding, L. Chen, Y. Chen, T. Zhou, H. Li, Y. Xu, L. Zhao, N. Huang, A facile, green synthesis of biomass carbon dots coupled with molecularly imprinted polymers for highly selective detection of oxytetracycline, J. Ind. Eng. Chem. 69 (2019) 455–463. https://doi.org/10.1016/J.JIEC.2018.10.007.

[13] S. Liu, Z. Liu, Q. Li, H. Xia, W. Yang, R. Wang, Y. Li, H. Zhao, B. Tian, Facile synthesis of carbon dots from wheat straw for colorimetric and fluorescent detection of fluoride and cellular imaging, Spectrochim. Acta Part A Mol. Biomol. Spectrosc. 246 (2021) 118964. https://doi.org/10.1016/J.SAA.2020.118964.

[14] H. Qi, M. Teng, M. Liu, S. Liu, J. Li, H. Yu, C. Teng, Z. Huang, H. Liu, Q. Shao, A. Umar, T. Ding, Q. Gao, Z. Guo, Biomass-derived nitrogen-doped carbon quantum dots: highly selective fluorescent probe for detecting Fe3+ ions and tetracyclines, J. Colloid Interface Sci. 539 (2019) 332–341. https://doi.org/10.1016/J.JCIS.2018.12.047.

[15] P. Roy, R. Ravindranath, A.P. Periasamy, C.W. Lien, C. Te Liang, H.T. Chang, Green synthesis of Si–GQD nanocomposites as cost-effective catalysts for oxygen reduction reaction, RSC Adv. 6 (2016) 108941–108947. https://doi.org/10.1039/C6RA23892K.

[16] M.P. Sk, A. Jaiswal, A. Paul, S.S. Ghosh, A. Chattopadhyay, Presence of

Amorphous Carbon Nanoparticles in Food Caramels, Sci. Rep. 2 (2012) 383. https://doi.org/10.1038/srep00383.

[17] C. Jiang, H. Wu, X. Song, X. Ma, J. Wang, M. Tan, Presence of photoluminescent carbon dots in Nescafe® original instant coffee: Applications to bioimaging, Talanta. 127 (2014) 68–74. https://doi.org/10.1016/J.TALANTA.2014.01.046.

[18] X. Zhang, H. Wang, C. Ma, N. Niu, Z. Chen, S. Liu, J. Li, S. Li, Seeking value from biomass materials: preparation of coffee bean shell-derived fluorescent carbon dots via molecular aggregation for antioxidation and bioimaging applications, Mater. Chem. Front. 2 (2018) 1269–1275. https://doi.org/10.1039/C8QM00030A.

[19] W. Zhang, L. Jia, X. Guo, R. Yang, Y. Zhang, Z. Zhao, Green synthesis of up- and down-conversion photoluminescent carbon dots from coffee beans for Fe3+ detection and cell imaging, Analyst. 144 (2019) 7421–7431. https://doi.org/10.1039/C9AN01953G.

[20] A. Maddu, R. Meliafatmah, E. Rustami, Enhancing Photocatalytic Degradationof Methylene Blue Using ZnO/Carbon DotsNanocomposite Derived From Coffee Grounds, Polish J. Environ. Stud. 30 (2020) 273–282. https://doi.org/10.15244/PJOES/120156.

[21] S.J. Park, H.K. Yang, Ultra-fast synthesis of carbon dots using the wasted coffee residues for environmental remediation, Curr. Appl. Phys. 36 (2022) 9–15. https://doi.org/10.1016/J.CAP.2022.01.001.

[22] M. Bottrill, L. Kwok, N.J. Long, Lanthanides in magnetic resonance imaging, Chem. Soc. Rev. 35 (2006) 557–571. https://doi.org/10.1039/B516376P.

[23] L. Pasquini, A. Napolitano, E. Visconti, D. Longo, A. Romano, P. Tomà, M.C.R. Espagnet, Gadolinium-Based Contrast Agent-Related Toxicities, CNS Drugs. 32 (2018) 229–240. https://doi.org/10.1007/S40263-018-0500-1.

[24] G.W. Kajjumba, M. Attene-Ramos, E.J. Marti, Toxicity of lanthanide coagulants assessed using four in vitro bioassays, Sci. Total Environ. 800 (2021). https://doi.org/10.1016/J.SCITOTENV.2021.149556.

[25] Y.-T.; Lin, R.-X.; Liu, G.; Audira, M.E.; Suryanto, M.J.M.; Roldan, Y.-T. Lin, R.-X. Liu, G. Audira, M.E. Suryanto, M. Jmelou, M. Roldan, J.-S. Lee, T.-R. Ger, C.-D. Hsiao, Lanthanides Toxicity in Zebrafish Embryos Are Correlated to Their Atomic Number, Toxics 2022, Vol. 10, Page 336. 10 (2022) 336. https://doi.org/10.3390/TOXICS10060336.

[26] C. Liu, D. Lu, X. You, G. Shi, J. Deng, T. Zhou, Carbon dots sensitized lanthanide infinite coordination polymer nanoparticles: Towards ratiometric fluorescent sensing of cerebrospinal Aβ monomer as a biomarker for Alzheimer's disease, Anal. Chim. Acta. 1105 (2020) 147–154. https://doi.org/10.1016/J.ACA.2020.01.021.

[27] J. Huang, W. Lu, J. Wang, Q. Li, B. Tian, C. Li, Z. Wang, L. Jin, J. Hao, Strategy to Enhance the Luminescence of Lanthanide Ions Doped MgWO4 Nanosheets through Incorporation of Carbon Dots, Inorg. Chem. 57 (2018) 8662–8672. https://doi.org/10.1021/ACS.INORGCHEM.8B01592/SUPPL_FILE/IC8B01592_SI_001.PDF.

[28] W. Sun, X. Han, F. Qu, R.M. Kong, Z. Zhao, A carbon dot doped lanthanide coordination polymer nanocomposite as the ratiometric fluorescent probe for the sensitive detection of alkaline phosphatase activity, Analyst. 146 (2021) 2862–2870. https://doi.org/10.1039/D1AN00218J.

[29] L. Wang, Y. Chen, Lanthanide doped carbon dots as a fluorescence chromaticity-based pH probe, Microchim. Acta 2018 18510. 185 (2018) 1–9. https://doi.org/10.1007/S00604-018-3027-8.

[30] M. Zhang, W. Wang, P. Yuan, C. Chi, J. Zhang, N. Zhou, Synthesis of lanthanum doped carbon dots for detection of mercury ion, multi-color imaging of cells and tissue, and bacteriostasis, Chem. Eng. J. 330 (2017) 1137–1147. https://doi.org/10.1016/J.CEJ.2017.07.166.

[31] A.C. Venu, R.N. Din, T. Rudszuck, P. Picchetti, P. Chakraborty, A.K. Powell, S. Krämer, G. Guthausen, M. Ibrahim, NMR Relaxivities of Paramagnetic Lanthanide-Containing Polyoxometalates, Molecules. 26 (2021). https://doi.org/10.3390/MOLECULES26247481.

[32] H. Chen, L. Wang, H. Fu, Z. Wang, Y. Xie, Z. Zhang, Y. Tang, Gadolinium functionalized carbon dots for fluorescence/magnetic resonance dual-modality imaging of mesenchymal stem cells, J. Mater. Chem. B. 4 (2016) 7472–7480. https://doi.org/10.1039/C6TB01422D.

[33] C. Yu, T. Xuan, Y. Chen, Z. Zhao, X. Liu, G. Lian, H. Li, Gadolinium-doped carbon dots with high quantum yield as an effective fluorescence and magnetic resonance bimodal imaging probe, J. Alloys Compd. 688 (2016) 611–619. https://doi.org/10.1016/J.JALLCOM.2016.07.226.

[34] Q. Jiang, L. Liu, Q. Li, Y. Cao, D. Chen, Q. Du, X. Yang, D. Huang, R. Pei, X. Chen, G. Huang, NIR-laser-triggered gadolinium-doped carbon dots for magnetic resonance imaging, drug delivery and combined photothermal chemotherapy for triple negative breast cancer, J. Nanobiotechnology. 19 (2021) 1–15. https://doi.org/10.1186/S12951-021-00811-W/TABLES/1.

[35] L. Wang, W. Zhou, D. Yang, H. Zhe, S. Mei, J. Yuan, W. Zhang, H. Li, H. Fan, F. Xie, R. Guo, Gadolinium-doped carbon dots with high-performance in dual-modal molecular imaging, Anal. Methods. 13 (2021) 2442–2449. https://doi.org/10.1039/D1AY00270H.

[36] N. Gong, H. Wang, S. Li, Y. Deng, X. Chen, L. Ye, W. Gu, Microwave-assisted polyol synthesis of gadolinium-doped green luminescent carbon dots as a bimodal nanoprobe, Langmuir. 30 (2014) 10933–10939. https://doi.org/10.1021/LA502705G/SUPPL_FILE/LA502705G_SI_001.PDF.

[37] A. Kharin, O. Syshchyk, A. Geloen, S. Alekseev, A. Rogov, V. Lysenko, V. Timoshenko, Carbon fluoroxide nanoparticles as fluorescent labels and sonosensitizers for theranostic applications, Http://Www.Tandfonline.Com/Action/JournalInformation?Show=aimsScope&journalCode=tsta20#.VmBmuzZFCUk. (2015). https://doi.org/10.1088/1468-6996/16/4/044601.

[38] H. Kuznietsova, N. Dziubenko, K. Pallienko, N. Pozdnyakova, N. Krisanova, A. Pastukhov, T. Lysenko, M. Dudarenko, V. Skryshevsky, V. Lysenko, T. Borisova, A comparative multi-level toxicity assessment of carbon-based Gd-free dots and Gd-doped nanohybrids from coffee waste: hematology, biochemistry, histopathology and neurobiology study, Sci. Reports 2023 131. 13 (2023) 1–14. https://doi.org/10.1038/s41598-023-36496-4.

[39] S. Fujita, M. Nakazawa, A. Hagiwara, R. Ueda, M. Horita, T. Maekawa, R. Irie, C. Andica, K.K. Kumamaru, M. Hori, S. Aoki, Estimation of Gadolinium-based Contrast Agent Concentration Using Quantitative Synthetic MRI and Its Application to Brain Metastases: A Feasibility Study, Magn. Reson. Med. Sci. 18 (2019) 260. https://doi.org/10.2463/MRMS.MP.2018-0119.

[40] A. Rajca, From High-Spin Organic Molecules to Organic Polymers with Magnetic Ordering, Chem. A Eu. 8 (2002) 4834–4841. https://chemistry-europe.onlinelibrary.wiley.com/doi/10.1002/1521-3765(20021104)8:21%3C4834::AID-CHEM4834%3E3.0.CO;2-E (accessed August 21, 2022).

[41] W. Fujita, K. Awaga, Room-Temperature Magnetic Bistability in Organic Radical Crystals, Science (80-.). 286 (1999) 261–262. https://doi.org/10.1126/SCIENCE.286.5438.261.

[42] L.M. Amzel, D.F. Covey, C. Fenselau, A. Nickon, C.H. Robinson, Organic structural analysis, John Wiley & Sons, Ltd, New York, NY, 1976. https://doi.org/10.1002/BMS.1200040612.

[43] S.H. Lam, H.Y. Hung, P.C. Kuo, D.H. Kuo, F.A. Chen, T.S. Wu, Application of Lanthanide Shift Reagent to the 1H-NMR Assignments of Acridone Alkaloids, Molecules. 25 (2020). https://doi.org/10.3390/MOLECULES25225383.

[44] Y. Wu, D.C. Xiong, S.C. Chen, Y.S. Wang, X.S. Ye, Total synthesis of mycobacterial arabinogalactan containing 92 monosaccharide units, Nat. Commun. 8 (2017). https://doi.org/10.1038/NCOMMS14851.

[45] A. V. Levdansky, N.Y. Vasilyeva, A.A. Kondrasenko, V.A. Levdansky, Y.N. Malyar, A.S. Kazachenko, B.N. Kuznetsov, Sulfation of arabinogalactan with sulfamic acid under homogeneous conditions in dimethylsulfoxide medium, Wood Sci. Technol. 55 (2021) 1725–1744. https://doi.org/10.1007/S00226-021-01341-2/TABLES/5.

[46] D.R.C. Junior, L.T. De Brito, F. Pocahy, I. Amaro, Melanoidins from Chinese Distilled Spent Grain: Content, Preliminary Structure, Antioxidant, and ACE-Inhibitory Activities In Vitro, Foods 2019, Vol. 8, Page 516. 8 (2019) 516. https://doi.org/10.3390/FOODS8100516.

[47] M. Kędzierska-Matysek, A. Matwijczuk, M. Florek, J. Barłowska, A. Wolanciuk, A. Matwijczuk, E. Chruściel, R. Walkowiak, D. Karcz, B. Gładyszewska, Application of FTIR spectroscopy for analysis of the quality of honey, BIO Web Conf. 10 (2018) 02008. https://doi.org/10.1051/BIOCONF/20181002008.

[48] R.J. Sammons, D.P. Harper, N. Labbé, J.J. Bozell, T. Elder, T.G. Rials, Characterization of organosolv lignins using thermal and FT-IR spectroscopic analysis,

BioResources. 8 (2013) 2752–2767. https://doi.org/10.15376/BIORES.8.2.2752-2767.

[49] D. Pujol, C. Liu, J. Gominho, M.À. Olivella, N. Fiol, I. Villaescusa, H. Pereira, The chemical composition of exhausted coffee waste, Ind. Crops Prod. 50 (2013) 423–429. https://doi.org/10.1016/J.INDCROP.2013.07.056.

[50] T. Hong, J.Y. Yin, S.P. Nie, M.Y. Xie, Applications of infrared spectroscopy in polysaccharide structural analysis: Progress, challenge and perspective, Food Chem. X. 12 (2021) 100168. https://doi.org/10.1016/J.FOCHX.2021.100168.

[51] A.S.P. Moreira, F.M. Nunes, M.R. Domingues, M.A. Coimbra, Coffee melanoidins: structures, mechanisms of formation and potential health impacts, Food Funct. 3 (2012) 903–915. https://doi.org/10.1039/C2FO30048F.

[52] H. Sharma, A Detail Chemistry of Coffee and Its Analysis, in: Coffee - Prod. Res., IntechOpen, 2020. https://doi.org/10.5772/intechopen.91725.

[53] A. Oosterveld, A.G.J. Voragen, H.A. Schols, Effect of roasting on the carbohydrate composition of Coffea arabica beans, Carbohydr. Polym. 54 (2003) 183–192. https://doi.org/10.1016/S0144-8617(03)00164-4.

[54] R.J. Redgwell, D. Curti, M. Fischer, P. Nicolas, L.B. Fay, Coffee bean arabinogalactans: Acidic polymers covalently linked to protein, Carbohydr. Res. 337 (2002) 239–253. https://doi.org/10.1016/S0008-6215(01)00316-0.

[55] Mauro Botta, Second Coordination Sphere Water Molecules and Relaxivity of Gadolinium(III) Complexes: Implications for MRI Contrast Agents , Eur. J. Inorg. Chem. 2000 (2000) 399–407. https://www.researchgate.net/publication/230135562_Second_Coordination_Sphere_Water_Molecules_and_Relaxivity_of_GadoliniumIII_Complexes_Implications_for_MRI_Contrast_Agents (accessed February 21, 2023).

[56] C. Robic, M. Port, O. Rousseaux, S. Louguet, N. Fretellier, S. Catoen, C. Factor, S. Le Greneur, C. Medina, P. Bourrinet, I. Raynal, J.M. Idée, C. Corot, Physicochemical and Pharmacokinetic Profiles of Gadopiclenol: A New Macrocyclic Gadolinium Chelate With High T1 Relaxivity, Invest. Radiol. 54 (2019) 475–484. https://doi.org/10.1097/RLI.0000000000000563.

[57] T.J. Clough, L. Jiang, K.L. Wong, N.J. Long, Ligand design strategies to increase stability of gadolinium-based magnetic resonance imaging contrast agents, Nat. Commun. 2019 101. 10 (2019) 1–14. https://doi.org/10.1038/s41467-019-09342-3.

[58] S.I.F.S. Martins, W.M.F. Jongen, M.A.J.S. Van Boekel, A review of Maillard reaction in food and implications to kinetic modelling, Trends Food Sci. Technol. 11 (2000) 364–373. https://doi.org/10.1016/S0924-2244(01)00022-X.

[59] N. Baccile, G. Laurent, F. Babonneau, F. Fayon, M.M. Titirici, M. Antonietti, Structural characterization of hydrothermal carbon spheres by advanced solid-state MAS 13C NMR investigations, J. Phys. Chem. C. 113 (2009) 9644–9654. https://doi.org/10.1021/JP901582X/SUPPL_FILE/JP901582X_SI_001.PDF.

[60] D. Cagniant, P. Magri, R. Gruber, S. Berlozecki, P.D. Saibut, J. Bimer, G. Nansé, Ammoxidation of cellulose—a structural study, J. Anal. Appl. Pyrolysis. 65 (2002) 1–23. https://doi.org/10.1016/S0165-2370(01)00172-3.

[61] N.L. Owen, Z. Pawlak, An infrared study of the effect of liquid ammonia on wood surfaces, J. Mol. Struct. 198 (1989) 435–449. https://doi.org/10.1016/0022-2860(89)80055-9.

[62] W. Wei, C. Xu, L. Wu, J. Wang, J. Ren, X. Qu, Non-enzymatic-browning-reaction: A versatile route for production of nitrogen-doped carbon dots with tunable multicolor luminescent display, Sci. Rep. 4 (2014) 1–7. https://doi.org/10.1038/srep03564.

[63] F.M. Nunes, M.A. Coimbra, Role of hydroxycinnamates in coffee melanoidin formation, Phytochem. Rev. 9 (2010) 171–185. https://doi.org/10.1007/S11101-009-9151-7/METRICS.

[64] M. Ginz, U.H. Engelhardt, Identification of Proline-Based Diketopiperazines in Roasted Coffee, J. Agric. Food Chem. 48 (2000) 3528–3532. https://doi.org/10.1021/JF991256V.

[65] R.J. Redgwell, C. Schmitt, M. Beaulieu, D. Curti, Hydrocolloids from coffee: physicochemical and functional properties of an arabinogalactan–protein fraction from green beans, Food Hydrocoll. 19 (2005) 1005–1015. https://doi.org/10.1016/J.FOODHYD.2004.12.010.

[66] E.K. Bekedam, Coffee brew melanoidins Structural and Functional Properties of Brown-Colored Coffee Compounds, 2008. https://edepot.wur.nl/122022 (accessed February 8, 2023).

CRediT authorship contribution statement

Konstantin Paliienko: Conceptualization, Data curation, Formal analysis, Investigation, Methodology, Visualization, Writing – original draft. **Anna Topchylo:** Investigation. **Sergei Alekseev:** Formal analysis, Writing - reviewing & editing. **Alain Géloën:** Investigation. **Yurii Milovanov:** Investigation. **Tetiana Lysenko:** Investigation. **Valeriy Skryshevsky:** Funding acquisition, Supervision. **Tatiana Borisova:** Conceptualization, Supervision. **Vladimir Lysenko:** Conceptualization, Data curation, Formal analysis, Supervision, Writing - reviewing & editing.